Journal of Power Sources 213 (2012) 63–68

Contents lists available at SciVerse ScienceDirect

Journal of Power Sources

journal homepage: www.elsevier.com/locate/jpowsour

Effects of pre-oxidation on the microstructural and electrical properties of $La_{0.67}Sr_{0.33}MnO_{3-\delta}$ coated ferritic stainless steels

Peng Yang [a,b], Chien-Kuo Liu [b], Jin-Yu Wu [c], Wei-Ja Shong [b], Ruey-Yi Lee [b], Chia-Chi Sung [a,*]

[a] Department of Engineering Science and Ocean Engineering, National Taiwan University, Taipei 10617, Taiwan, ROC
[b] Nuclear Fuels and Materials Division, Institute of Nuclear Energy Research, Longtan, Taoyuan 32546, Taiwan, ROC
[c] Physics Division, Institute of Nuclear Energy Research, Longtan, Taoyuan 32546, Taiwan, ROC

ARTICLE INFO

Article history:
Received 23 December 2011
Received in revised form
20 March 2012
Accepted 21 March 2012
Available online 19 April 2012

Keywords:
Solid oxide fuel cells (SOFCs)
Interconnect
Protective layer
Pre-oxidation
Area specific resistance (ASR)

ABSTRACT

$La_xSr_{1-x}MnO_3$ (LSM) is commonly used as a protective layer on the metallic interconnects of solid oxide fuel cells (SOFCs) to prevent surface oxidation and chromium poisoning. However, the volume shrinkage at elevated temperatures causes the LSM coatings to crack, resulting in chromium diffusion. Therefore, this paper investigates the effects of pre-oxidation on the microstructure and electrical properties of ferritic stainless steels coated with $La_{0.67}Sr_{0.33}MnO_3$ (LSM). Four ferritic stainless steels were selected for use as interconnect substrates: Crofer22APU, Crofer22H, ss441, and ZMG232L. The candidate materials were pre-oxidised at 850 °C for 25 and 50 h, respectively. After the pre-oxidation process, the LSM films with a thickness of 3–4 μm were deposited on the surface of samples by using Pulsed DC magnetron sputtering. After aging the coated specimens at elevated temperatures, the morphologies and crystalline structures were examined using SEM/EDX and XRD, respectively. The results indicated that the pre-oxidised layer, $(Mn, Cr)_3O_4$, could significantly suppress chromium penetration from the interior to the surface of the specimens. Moreover, the area specific resistance (ASR) values for the 25-h pre-oxidised specimens were 2.24, 12.21, 2.30, and 6.77 mΩ cm^2 for Crofer22APU, Crofer22H, ss441, and ZMG232L, respectively, at 800 °C for 500 h in an air atmosphere.

1. Introduction

Ferritic Stainless Steels (e.g., Crofer22APU) are commonly used as interconnects for solid oxide fuel cells (SOFCs) because of advantages such as relatively low cost, easy fabrication, high electronic conductivity and low ion conductivity [1–7]. In addition, "Yang et al. [8] pointed out that the coefficient of thermal expansion (CTE) of ferritic stainless steels and austenitic stainless steels are typically in the range of $11.5–14.0 \times 10^{-6}\,K^{-1}$ and $18.0–20.0 \times 10^{-6}\,K^{-1}$, respectively, at the range of temperature from room temperature to 800 °C. Metallic interconnect used in the SOFC stack must adhere to both the ceramic positive cathode–electrolyte–negative anode (PEN) plate and seal materials such as glass-ceramic. The CTE of PEN is typically in the range of $10.5–12.5 \times 10^{-6}\,K^{-1}$. Therefore, ferritic stainless steels match other adjacent components better than austenitic stainless steels. However, long-term exposure of metallic interconnects to high temperatures under an oxidant atmosphere results in the formation of oxide scales, such as Cr_2O_3, which increases the electrical contact resistance to electrodes and reduces the electrochemical performance of SOFCs. Moreover, Cr can be released from these chromium oxides and react with moisture to form volatile $CrO_2(OH)_2$, which poisons the cathode and the cathode/electrolyte interface, and further degrades the performance of the fuel cells [9–12]. Consequently, recent trends in the development of metallic interconnects is moving toward depositing a protective coating on the interconnect surfaces to improve its oxidation resistance over the service lifetime [13–22]. Various studies have been conducted using Pulsed DC magnetron sputtering to deposit a $La_xSr_{1-x}MnO_3$ (LSM)-based perovskite ceramic film as an effective coating for SOFC applications. However, after post heat treatment such as calcination or annealing at elevated temperatures, cracks could be formed on the surface of the protective coating due to phase transformation and volume shrinkage of the LSM film from amorphous to crystalline [23,24]. Chu et al. [25,26] also found that cracks were generated on the surface of LSM thin film due to the shrinkage of thin film during cooling after the pulsed DC magnetron sputtering process. After a period of exposure to a hot air atmosphere, $(Mn, Cr)_3O_4$ spinels were generated along the cracks due to the Cr elements evaporating from the substrate and then combining with Mn in the LSM thin film to form $(Mn, Cr)_3O_4$ spinels.

* Corresponding author. Tel.: +886 2 33665769; fax: +886 2 23929885.
E-mail address: ccsung@ntu.edu.tw (C.-C. Sung).

0378-7753/$ – see front matter © 2012 Elsevier B.V. All rights reserved.
doi:10.1016/j.jpowsour.2012.03.054

A possible solution to treat this problem is to suppress the Cr elements evaporating from the surface of the steel by forming a $(Mn, Cr)_3O_4$ layer with the pre-oxidation treatment. Macauley et al. [27] studied the influence of pre-treatment on the oxidation behavior of Co coated ss441 used as SOFC interconnect. Their results showed that the significant differences in oxidation behavior were observed. Furthermore, Holcomb et al. [28,29] reported that the maximum evaporation rate of Cr elements from Cr_2O_3 is higher than that form $(Mn, Cr)_3O_4$, and the reduction in Cr evaporation factor is 35 for $(Mn, Cr)_3O_4$ spinel at 800 °C. In this study, we focused on the microstructural and electrical properties of LSM-coated films that were deposited on pre-oxidised Crofer22APU, Crofer22H, ss441, and ZMG232L substrates after isothermal aging at 800 °C for 500 h. In the present paper, the different coating/substrate specimens were first characterised by XRD to identify their structures and, subsequently, to estimate the ability of Cr migration. Surface morphologies were used to evaluate the adherence of the metal/scale interface. Finally, the ASR values were measured.

2. Experimental procedures

2.1. Sample preparation

Four commercial ferritic stainless steels, Crofer22APU, Crofer22H, ss441, and ZMG232L, obtained from ThyssenKrupp VDM, Germany, Nippon Steel Co., Japan, and Hitachi Metals, Ltd., Japan, were employed in this study. The compositions of the ferritic stainless steels, which were provided by the suppliers, are listed in Table 1. The as-received sheets were cut into 10×10 mm^2 coupons, polished with SiC papers ranging up to 1200 grit, and cleaned before further treatment. The four ferritic stainless steel coupons of without pre-oxidation and with pre-oxidised treatment were used as substrates. Prior to coating, the four ferritic stainless steel coupons were pre-oxidised at 850 °C for 25 and 50 h in an electric furnace under air flowing at 2×10^{-3} m^3 min^{-1}. The heating rate was 5 °C min^{-1}.

2.2. LSM coating

An amorphous LSM film was deposited on the surfaces of the steel samples using a pulsed DC magnetron sputter coater (see Fig. 1) at 1.5 kW of power. A high purity (99.9%) of $La_{0.67}Sr_{0.33}MnO_3$ bulk (in sintered form) was used as sputter target for the coating process in this study. The distance between the specimens and the target was 5 cm. Sputter coating was performed in an Argon atmosphere at a pressure of 0.99 Pa and a flow rate of 0.22 Pa m^3 s^{-1}. The thickness of the LSM film was approximately 3–4 μm.

2.3. XRD analysis

The crystalline structures of the LSM coatings of the as-coated specimens were analysed by the grazing incident diffraction technique using an X-ray diffractometer (D8 Discover, Bruker, Germany) equipped with Cu K_α (1.5406 Å) radiation. The XRD measurement was conducted at an operating voltage of 40 kV and a current of 40 mA. The scanning range was 2θ=15°–85°; the scanning speed was 4° min^{-1}; and the grazing angle α was 2°.

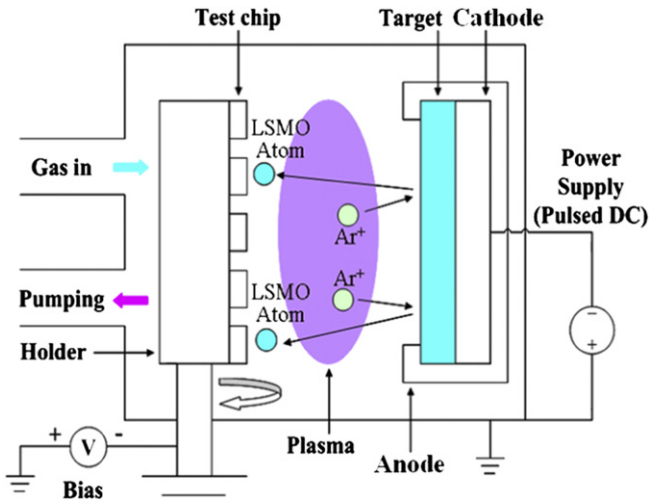

Fig. 1. Schematic diagram of pulsed DC magnetron sputtering system.

2.4. SEM microstructure observation

The surface morphologies and elemental compositions of the LSM coatings were investigated using a field emission scanning electron microscopy (FE-SEM) (Hitachi S4800I, Japan) equipped with an energy dispersive X-ray spectrometer (EDX) (Horiba, Japan). An acceleration voltage of 15 kV and secondary electron imaging were employed during the observations.

2.5. ASR measurement

The area specific resistance (ASR) measurements were carried out using the standard DC four-point technique [4,29–32]. Silver paste was used as contact paste for the ASR measurements. The coated and un-coated specimens were placed into an electric furnace and isothermally aged at 800 °C for 500 h in an atmosphere of humid air (−3%) with a flow rate of 2×10^{-3} m^3 min^{-1}. The ASR tests were conducted at a constant current of 140 mA using a Keithley 2400 system. The variations in resistance were monitored and calculated using the Keithley 2700 system.

3. Results and discussion

The XRD patterns of the LSM film coated on Crofer22APU, Crofer22H, ss441, and ZMG232L after aging at 800 °C for 500 h in an air atmosphere are shown in Fig. 2(a)–(d). After aging at 850 °C for 4 h, the crystalline structure of as-coated LSMO film transformed from the amorphous phase to the perovskite phase. The $(Mn, Cr)_3O_4$ spinels can be deposited on the surface of LSM layer due to Cr element evaporating from inner substrate and combining with Mn

Table 1
Compositions of Crofer22APU, Crofer22H, ss441, and ZMG232L (in wt.%).

Alloys	Fe	Cr	Mn	Si	Cu	Al	S	P	Ti	La	Nb	Ni	Zr	C
Crofer22APU	Bal.	20–24	0.3–0.8	≦0.50	≦0.50	≦0.50	≦0.02	≦0.05	0.03–0.20	0.04–0.20	–	–	–	≦0.03
Crofer22H	Bal.	20–24	0.3–0.8	0.1–0.60	≦0.50	≦0.10	≦0.03	≦0.03	0.02–0.20	0.04–0.20	0.20–0.10	–	–	≦0.03
ss441	Bal.	18	0.35	≦0.34	–	≦0.05	≦0.02	≦0.023	0.22	–	0.5	0.3	–	≦0.01
ZMG232L	Bal.	21–23	≦0.10	≦0.10	–	≦0.50	≦0.03	≦0.03	–	0.03–0.10	–	≦0.70	0.10–0.40	≦0.10

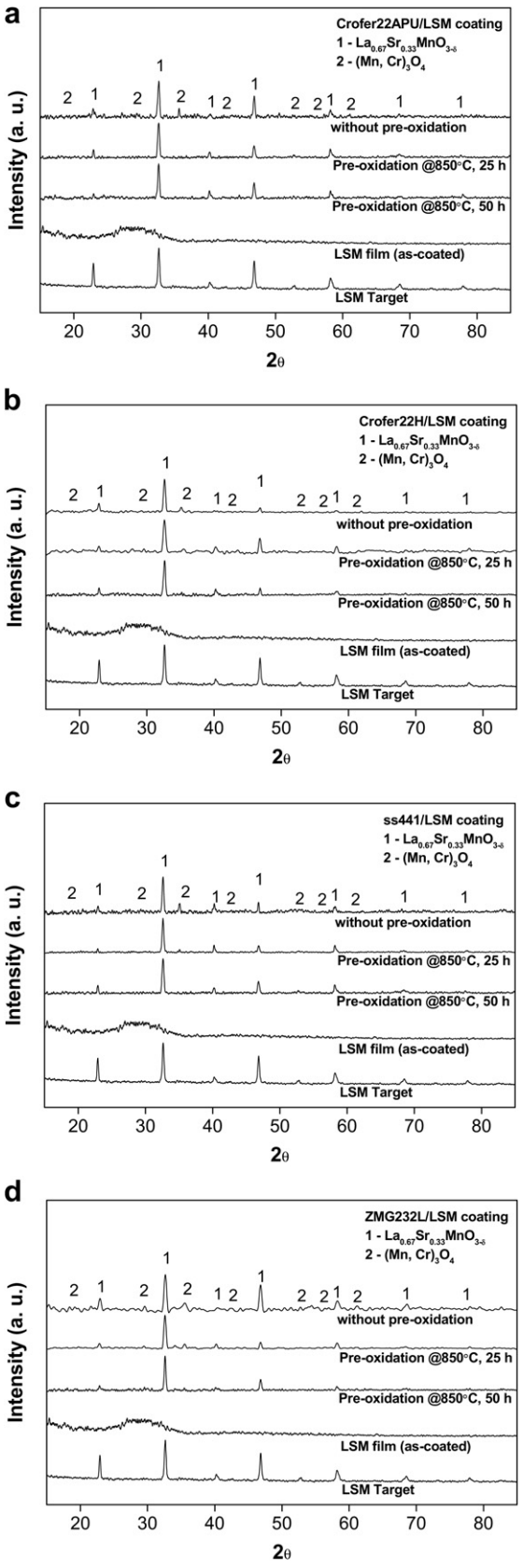

Fig. 2. XRD patterns of LSM-coated (a) Crofer22APU; (b) Crofer22H, (c) ss441; and (d) ZMG232L after aging at 800 °C for 500 h in air. (Note: substrates were prepared with different pre-oxidation conditions.)

to form oxides after long-term exposure to an hot air atmosphere. However, in Fig. 2(a)–(d), comparing the characteristic peaks of the $(Mn, Cr)_3O_4$ spinels (e.g. 2θ=37.38°) on the surfaces of the specimens, the substrate did not undergo the pre-oxidation treatment is more pronounced than that received the pre-oxidation treatment. This finding implies that the $(Mn, Cr)_3O_4$ pre-oxidised layer efficiently suppressed Cr diffusion toward the outer surface.

Froitzheim et al. [7] reported that the differences in oxide scale morphologies and alloy microstructures of the Crofer22APU and Crofer22H after 1000 h discontinuous oxidation at 900 °C in air. They found that in all of the cases the oxide scale consisted of an outer $(Mn, Cr)_3O_4$ layer and an inner Cr_2O_3 layer. An internal oxidation zone of Ti oxides formed beneath the surface of Crofer22APU and Crofer22H. However, the Laves phases comprised of W, Nb, and Si can only be seen in Crofer22H. Fig. 3(a)–(l) show the SEM cross-sectional micrographs of the pre-oxidised Crofer22APU, Crofer22H, ss441, and ZMG232L specimens at different oxidation times and then with the LSM coating after aging at 800 °C for 500 h in air. The images show that there is an oxidation scale, which consists of an outer $(Mn, Cr)_3O_4$ layer and an inner Cr_2O_3 layer, between the metallic substrate and the film coating. In addition, it can be found that the TiO_2 formed beneath the surface of the ferritic stainless steels used in the present study. However, the Laves phase can only be found in Crofer22H and ss441 due to Nb addition in the composition. Shong et al. [33] showed that the Lanthanum-based perovskite coatings such as $La_{0.8}Ca_{0.2}CrO_3$, $La_{0.8}Sr_{0.2}CrO_3$, and $La_{0.8}Sr_{0.2}MnO_3$ could facilitate the growth of the $(Mn, Cr)_3O_4$ spinel phase of the oxide scale of Crofer22APU with coarser crystalline structure and higher levels of Mn content. Comparing Fig. 3(a)–(l) reveals that the thickness of the oxidation layer of LSM-coated Crofer22H is thicker than that of the oxidation layers on Crofer22APU, ss441 and ZMG232L. The thickness of the oxidation layer is also one of the sources of the area specific resistance of the metallic substrate/LSM coating system.

Fig. 4(a)–(l) is the SEM micrographs of the surface morphologies of the pre-oxidised Crofer22APU, Crofer22H, ss441, and ZMG232L specimens at different oxidation times, followed by those with the LSM coating after aging at 800 °C for 500 h in air. After calcination at elevated temperatures, it was possible to generate crevices on the surface of LSM film. Also, chromium can diffuse from the substrate and thus grow $(Mn, Cr)_3O_4$ spinels along the crevices on the surface of LSM film. However, fewer $(Mn, Cr)_3O_4$ spinels can be found along the crevices of the specimens with the pre-oxidised substrate/LSM coating, as is shown in Fig. 4(b), (c), (e), (f), (h), (i), (k) and (l). This is attributed to a thin $(Mn, Cr)_3O_4$ oxide layer that formed after the pre-oxidation treatment, and this oxide layer effectively prevented the diffusion of chromium from the substrate. According to a report by Holcomb and Alman [28,29], the loss rate of chromium from Cr_2O_3 is 35 times higher than that from $MnCr_2O_4$ at 800 °C under either dry air conditions or air with 5% H_2O.

The evolution of the ASR values of the LSM-coated Crofer22APU, Crofer22H, ss441, and ZMG232L specimens at 800 °C for 500 h in air are shown in Fig. 5(a)–(d), respectively. Each substrate was respectively pre-oxidised at 850 °C for 25 and 50 h. Because the LSM-coated Crofer22APU specimens had the thinnest oxidation layers, they also have a relatively low ASR value. The initial values for the specimens with LSM coated on pre-oxidised substrates are higher than for the LSM/non-pre-oxidised substrate specimens. However, the corresponding increments of ASR values for the LSM/pre-oxidised substrate specimens are lower than for the LSM/non-pre-oxidised substrate specimens, after aging at 800 °C for 500 h. In the present study, the increment ratio of ASR for Crofer22APU with pre-oxidation at 850 °C for 50 h, 25 h, and without pre-oxidation are 4.06% (1.97–2.05 mΩ cm^2), 26.55% (1.77–2.24 mΩ cm^2), and 57.14% (1.05–1.65 mΩ cm^2), respectively.

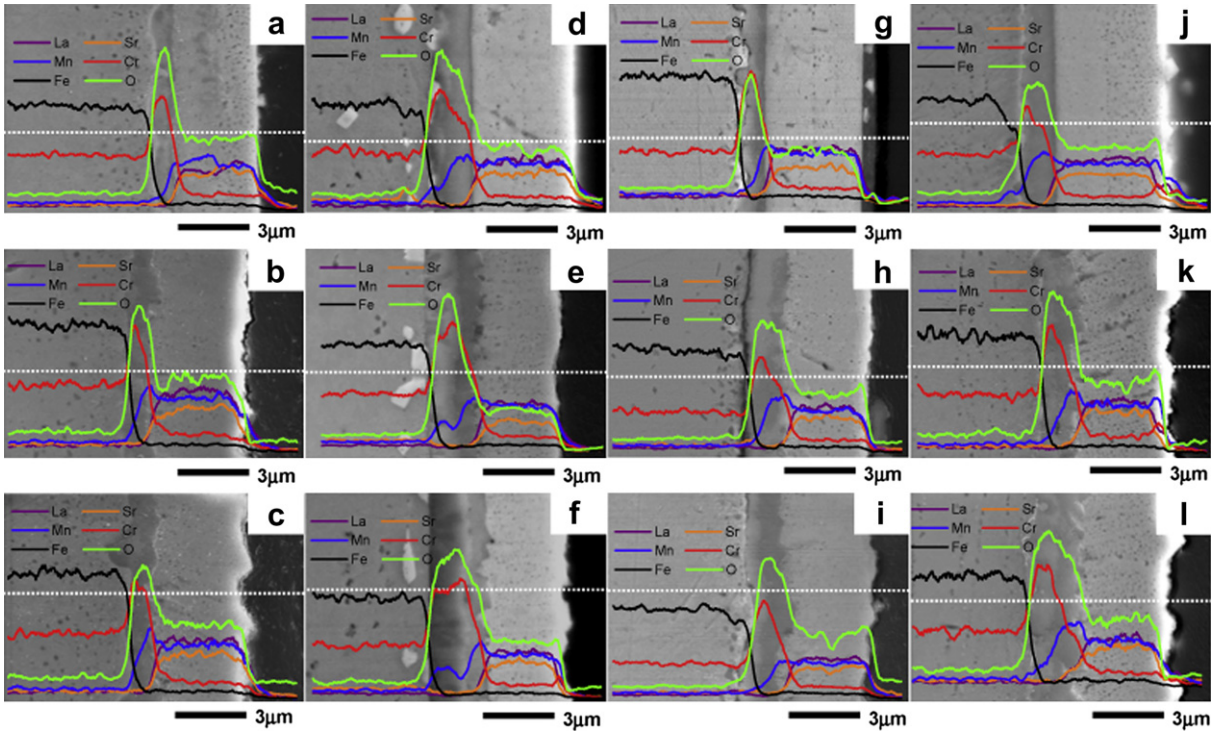

Fig. 3. Cross-section SEM micrographs of LSM-coated (a)–(c) Crofer22APU; (d)–(f) Crofer22H, (g)–(i) ss441 and (j)–(l) ZMG232L after aging at 800 °C for 500 h in air. The substrate's condition was (a) without pre-oxidation; (b) pre-oxidised at 850 °C for 25 h in air; and (c) pre-oxidised at 850 °C for 50 h in air, respectively. (Note: substrate's conditions of (d)–(f), (g)–(i) and (j)–(l) are the same as (a)–(c) in sequence.)

This is attributed to the fact that the pre-oxidised layer, $(Mn, Cr)_3O_4$, can effectively inhibit the outward diffusion of Cr element, thus reducing the growth rate of the oxide thickness.

From the results of the ASR measurements, the activation energy of electrical conductivity in the substrate/coating system can be calculated. The electrical conductivity of the LSM film is a thermally activated process and is a function of inverse temperature. The kinetics can be expressed as [34–37]:

$$\frac{T}{\mathrm{ASR}} = A_0 \exp\left(\frac{-E_a}{RT}\right) \quad (1)$$

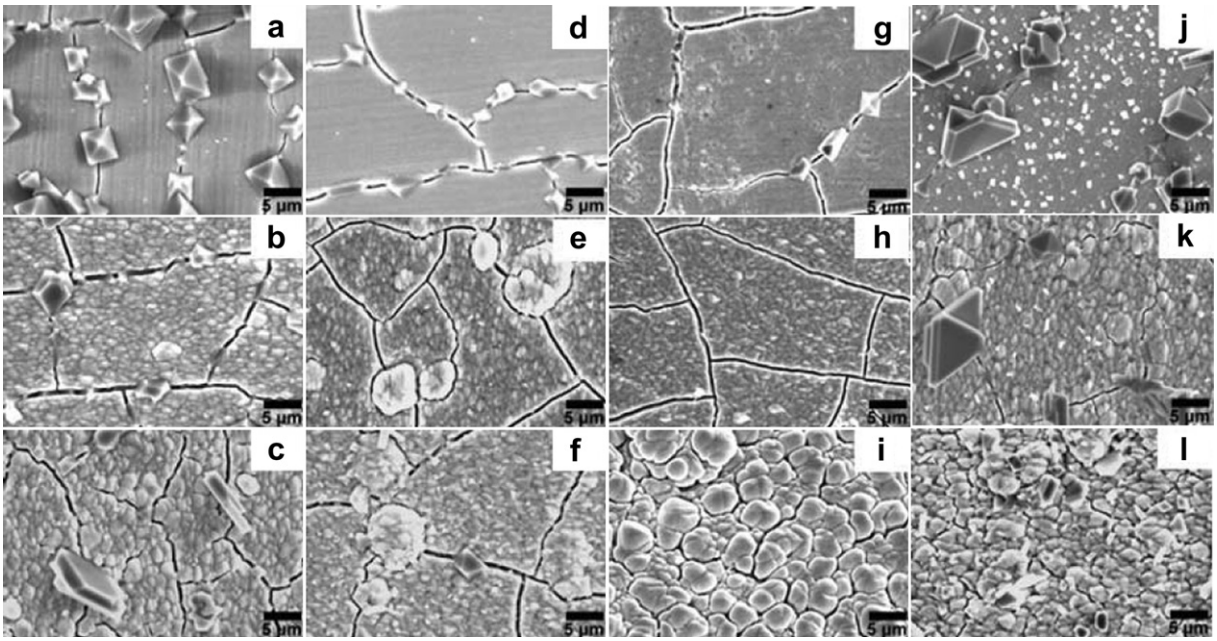

Fig. 4. SEM micrographs (surface morphologies) of LSM-coated (a)–(c) Crofer22APU; (d)–(f) Crofer22H, (g)–(i) ss441 and (j)–(l) ZMG232L after aging at 800 °C for 500 h in air. The substrate's condition was (a) without pre-oxidation; (b) pre-oxidised at 850 °C for 25 h in air; and (c) pre-oxidised at 850 °C for 50 h in air, respectively. (Note: substrate's conditions of (d)–(f), (g)–(i) and (j)–(l) are the same as (a)–(c) in sequence.)

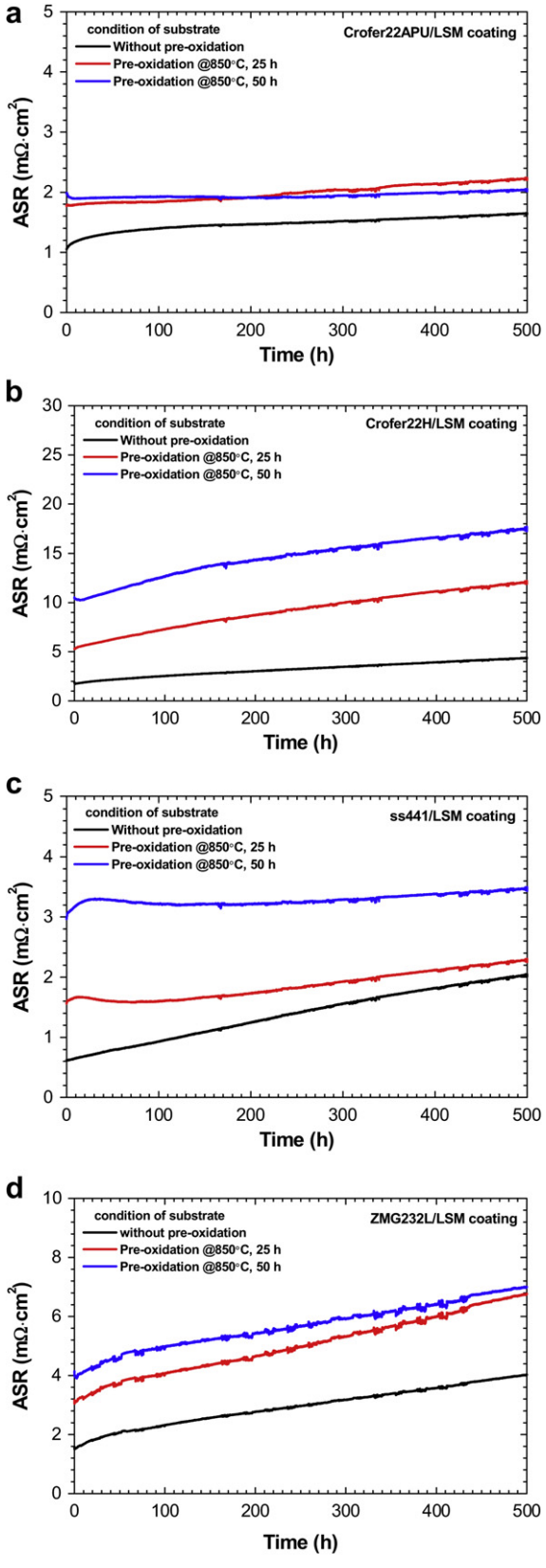

Fig. 5. Area specific resistance (ASR) values of LSM-coated (a) Crofer22APU; (b) Crofer22H, (c) ss441; and (d) ZMG232L after aging at 800 °C for 500 h in air. (Note: substrates were prepared with different pre-oxidation conditions.)

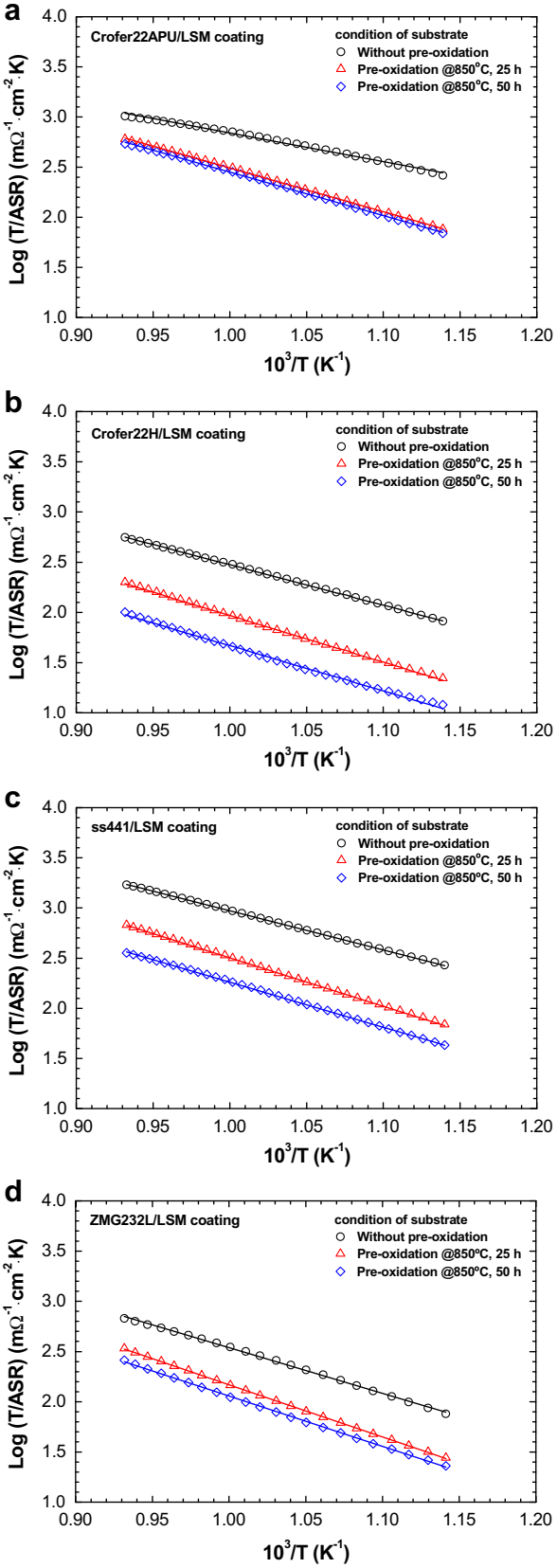

Fig. 6. Arrhenius plots of LSM-coated (a) Crofer22APU; (b) Crofer22H, (c) ss441; and (d) ZMG232L during heating at elevated temperatures in air.

Table 2
The activation energies of the LSM-coated ferritic stainless steels.

Substrate/coating	Activation energy (kJ mol^{-1})[a]		
	Pre-treatment of substrate		
	Without pre-oxidation	Pre-oxidation at 800 °C for 25 h	Pre-oxidation at 800 °C for 50 h
Crofer22APU/LSM	54.03	82.98	82.98
Crofer22H/LSM	77.19	88.77	86.84
ss441/LSM	74.29	92.63	85.87
ZMG232L/LSM	86.84	99.38	96.49

[a] Calculated temperature range: 600–800 °C.

T is the absolute temperature; E_a is the activation energy; R is the gas constant; and A_0 is a constant. The activation energy is obtained by plotting Eq. (1). Fig. 6(a)–(d) shows the Arrhenius plots of the LSM-coated Crofer22APU, Crofer22H, ss441, and ZMG232L specimens at elevated temperatures. The slope of the linear fitting line indicates the quantity of the activation energy. The activation energies of the specimens with LSM coated on bare substrates (Crofer22APU, Crofer22H, ss441, and ZMG232L) are 54.03, 77.19, 74.29, and 86.84 kJ mol^{-1}, respectively. The activation energies of the specimens with LSM coated on pre-oxidised substrates are listed in Table 2. The activation energies of the LSM/pre-oxidised substrates are slightly higher than those of the LSM/bare substrate. Again, this can be attributed to the thicker pre-oxidised layer and the lower electrical conductivity.

4. Conclusions

The effects of pre-oxidation on the microstructural and electrical properties of LSM-coated Crofer22APU, Crofer22H, ss441, and ZMG232L have been investigated in this study. Dense and uniform LSM films with thicknesses of 3–4 μm were successfully deposited on the surfaces of the pre-oxidised interconnect substrates using Pulsed DC magnetron sputtering. Although the crevices in the LSM coatings could easily be generated by the volume shrinkage resulting from the phase transformation during aging at elevated temperatures, the preliminary results of this study showed that the pre-oxidation treatment significantly suppresses the penetration of chromium from the interior to the surface of the specimens. This may be attributed to the retardation of chromium diffusion by the pre-oxidised layer, $(Mn, Cr)_3O_4$, formed after pre-oxidation. In addition, the results of the ASR measurements showed that the corresponding increments of the ASR values for the specimens with LSM coated on pre-oxidised substrates are lower than for the specimens of LSM/non-pre-oxidised substrates after aging at 800 °C for 500 h. In this paper, we have illustrated that the pre-oxidation treatment is a simple and effective way to inhibit the diffusion of Cr element from the oxide scale to the surface, and it lowers the increasing rate of ASR during aging at high temperatures. For instance, the initial ASR values for the LSM-coated Crofer22APU, Crofer22H, ss441, and ZMG232L specimens, respectively, which were pre-oxidised at 850 °C for 25 h, were 1.77, 5.31, 1.56, and 3.17 mΩ cm^2 and increased to 2.24, 12.21, 2.30, and 6.77 mΩ cm^2 after aging at 800 °C for 500 h, respectively. Furthermore, in this study, we showed that the LSM-coated specimen with the pre-oxidation treatment had a stronger effect on the resistance of Cr diffusion than that of the LSM-coated specimen without the pre-oxidation treatment.

Acknowledgment

The authors would like to thank Hitachi Metals Ltd. for kind offering ZMG232L for testing.

References

[1] J.W. Fergus, Mater. Sci. Eng. A 397 (2005) 271–283.
[2] J.A. Scott, D.C. Dunand, Acta Mater. 58 (2010) 6125–6133.
[3] H.S. Seo, G. Jin, J.H. Jun, D.H. Kim, K.Y. Kim, J. Power Sources 178 (2008) 1–8.
[4] S.J. Geng, J.H. Zhu, Z.G. Lu, Solid State Ionics 177 (2006) 559–568.
[5] P.D. Jablonski, C.J. Cowen, J.S. Sears, J. Power Sources 195 (2010) 813–820.
[6] M. Han, S. Peng, Z. Wang, Z. Yang, X. Chen, J. Power Sources 164 (2007) 278–283.
[7] J. Froitzheim, G.H. Meier, L. Niewolak, P.J. Ennis, H. Hattendorf, L. Singheiser, W.J. Quadakkers, J. Power Sources 178 (2008) 163–173.
[8] Z. Yang, K.S. Weil, D.M. Paxton, J.W. Stevenson, J. Electrochem. Soc. 150 (2003) A1188–A1201.
[9] K. Hilpert, D. Das, M. Miller, D.H. Peck, R. Weiss, J. Electrochem. Soc. 143 (1996) 3642–3647.
[10] J.W. Fergus, Int. J. Hydrogen Energy 32 (2007) 3664–3671.
[11] P.D. Jablonski, D.E. Alman, J. Power Sources 180 (2008) 433–439.
[12] B. Hua, J. Pu, F. Lu, J. Zhang, B. Chi, L. Jian, J. Power Sources 195 (2010) 2782–2788.
[13] A. Balland, P. Gannon, M. Deibert, S. Chevalier, G. Caboche, S. Fontana, Surf. Coat. Technol. 203 (2009) 3291–3296.
[14] X. Chen, B. Hua, J. Pu, J. Li, L. Zhang, S.P. Jiang, Int. J. Hydrogen Energy 34 (2009) 5737–5748.
[15] Q.X. Fu, D. Sebold, F. Tietz, H.P. Buchkremer, Solid State Ionics 192 (2011) 376–382.
[16] X. Montero, F. Tietz, D. Sebold, H.P. Buchkremer, A. Ringuede, M. Cassir, A. Laresgoiti, I. Villarreal, J. Power Sources 184 (2008) 172–179.
[17] X. Montero, F. Tietz, D. Stöver, M. Cassir, I. Villarreal, J. Power Sources 188 (2009) 148–155.
[18] S.S. Pyo, S.B. Lee, T.H. Lim, R.H. Song, D.R. Shin, S.H. Hyun, Y.S. Yoo, Int. J. Hydrogen Energy 36 (2011) 1868–1881.
[19] N. Shaigan, W. Qu, D.G. Ivey, W. Chen, J. Power Sources 195 (2010) 1529–1542.
[20] Y. Liu, D.Y. Chen, Int. J. Hydrogen Energy 34 (2009) 9220–9226.
[21] J. Wu, C.D. Johnson, R.S. Gemmen, X. Liu, J. Power Sources 189 (2009) 1106–1113.
[22] J. Wu, C. Li, C. Johnson, X. Liu, J. Power Sources 175 (2008) 833–840.
[23] N. Orlovskaya, A. Coratolo, C. Johnson, R. Gemmen, J. Am. Ceram. Soc. 87 (2004) 1981–1987.
[24] D.J. Jan, C.T. Lin, C.F. Ai, Thin Solid Films 516 (2008) 6300–6304.
[25] C.L. Chu, J.Y. Wang, S. Lee, Int. J. Hydrogen Energy 33 (2008) 2536–2546.
[26] C.L. Chu, J. Lee, T.H. Lee, Y.N. Cheng, Int. J. Hydrogen Energy 34 (2009) 422–434.
[27] C. Macauley, P. Gannon, M. Deibert, P. White, Int. J. Hydrogen Energy 36 (2011) 4540–4548.
[28] G.R. Holcomb, D.E. Alman, J. Mater. Eng. Perform. 15 (2006) 394–398.
[29] G.R. Holcomb, D.E. Alman, Scr. Mater. 54 (2006) 1821–1825.
[30] P. Piccardo, P. Gannon, S. Chevalier, M. Viviani, A. Barbucci, G. Caboche, R. Amendola, S. Fontana, Surf. Coat. Technol. 202 (2007) 1221–1225.
[31] S. Fontana, R. Amendola, S. Chevalier, P. Piccardo, G. Caboche, M. Viviani, R. Molins, M. Sennour, J. Power Sources 171 (2007) 652–662.
[32] Z. Yang, G.G. Xia, J.W. Stevenson, J. Power Sources 160 (2006) 1104–1110.
[33] W.J. Shong, C.K. Liu, C.Y. Chen, C.C. Peng, H.J. Tu, G.T.K. Fey, R.Y. Lee, H.M. Kao, Mater. Chem. Phys. 127 (2011) 45–50.
[34] Z. Lu, J. Zhu, E.A. Payzant, M.P. Paranthaman, J. Am. Ceram. Soc. 88 (2005) 1050–1053.
[35] H. Ebrahimifar, M. Zandrahimi, Solid State Ionics 183 (2011) 71–79.
[36] X. Zhou, P. Wang, L. Liu, K. Sun, Z. Gao, N. Zhang, J. Power Sources 191 (2009) 377–383.
[37] X. Chen, P.Y. Hou, C.P. Jacobson, S.J. Visco, L.C. De Jonghe, Solid State Ionics 176 (2005) 425–433.